



HAL
open science

Fuzzy Static Output Feedback Control for Path Following of Autonomous Vehicles With Transient Performance Improvements

Tran Anh-Tu Nguyen, Chouki Sentouh, Hui Zhang, Jean-Christophe Popieul

► **To cite this version:**

Tran Anh-Tu Nguyen, Chouki Sentouh, Hui Zhang, Jean-Christophe Popieul. Fuzzy Static Output Feedback Control for Path Following of Autonomous Vehicles With Transient Performance Improvements. IEEE Transactions on Intelligent Transportation Systems, 2020, 21 (7), pp.3069-3079. 10.1109/TITS.2019.2924705 . hal-03468394

HAL Id: hal-03468394

<https://uphf.hal.science/hal-03468394>

Submitted on 25 Nov 2023

HAL is a multi-disciplinary open access archive for the deposit and dissemination of scientific research documents, whether they are published or not. The documents may come from teaching and research institutions in France or abroad, or from public or private research centers.

L'archive ouverte pluridisciplinaire **HAL**, est destinée au dépôt et à la diffusion de documents scientifiques de niveau recherche, publiés ou non, émanant des établissements d'enseignement et de recherche français ou étrangers, des laboratoires publics ou privés.

See discussions, stats, and author profiles for this publication at: <https://www.researchgate.net/publication/334404544>

Fuzzy Static Output Feedback Control for Path Following of Autonomous Vehicles With Transient Performance Improvements

Article in *IEEE Transactions on Intelligent Transportation Systems* · July 2020

DOI: 10.1109/TITS.2019.2924705

CITATIONS

66

READS

470

4 authors, including:



Anh-Tu Nguyen

Université Polytechnique Hauts-de-France

140 PUBLICATIONS 2,084 CITATIONS

[SEE PROFILE](#)



Chouki Sentouh

LAMIH UMR CNRS 8201 Hauts-de-France Polytechnic University

114 PUBLICATIONS 2,057 CITATIONS

[SEE PROFILE](#)

Fuzzy Static Output Feedback Control for Path Following of Autonomous Vehicles with Transient Performance Improvements

Anh-Tu Nguyen*, *Member, IEEE*, Chouki Sentouh, *Member, IEEE*, Hui Zhang, *Senior Member, IEEE*, and Jean-Christophe Popieul

Abstract—This paper provides a new solution for path following control of autonomous ground vehicles. \mathcal{H}_2 control problem is considered to attenuate the effect of the road curvature disturbance. To this end, we formulate a standard model from the road-vehicle dynamics, the *a priori* knowledge on the road curvature, and the path following specifications. This standard model is then represented in a Takagi-Sugeno fuzzy form to deal with the time-varying nature of the vehicle speed. Based on a static output feedback scheme, the proposed method allows avoiding expensive vehicle sensors while keeping the simplest control structure for real-time implementation. The concept of \mathcal{D} -stability is exploited using Lyapunov stability arguments to improve the transient behaviors of the closed-loop vehicle system. In particular, the physical upper and lower bounds of the vehicle acceleration are explicitly considered in the design procedure via a parameter-dependent Lyapunov function to reduce drastically the design conservatism. The proposed \mathcal{H}_2 design conditions are expressed in terms of linear matrix inequalities (LMIs) with a single line search parameter. The effectiveness of the new path following control method is clearly demonstrated with both theoretical illustrations and hardware experiments under real-world driving situations.

Index Terms—Autonomous vehicles, path following, vehicle dynamics control, fuzzy static output feedback control, \mathcal{D} -stability.

I. INTRODUCTION

Autonomous ground vehicles have become a major focus of today's automotive industry and academia [1], [2]. This has been motivated by two factors. First, over the years traffic statistics have shown a raising number of fatal road accidents, of which an estimation of 94% are caused by driver errors [3]. Second, recent advances in sensing technology, data processing and telecommunication enable the developments of driverless driving technology [1]. Apart from reducing dramatically the human driver's mistakes, autonomous vehicles provide a great freedom for everyday travels, especially for people with physical or visual disability.

This work is supported by the French Ministry of Higher Education and Research, the National Center for Scientific Research (CNRS), the Nord-Pas-de-Calais Region under the project ELSAT 2020. Hui Zhang was supported in part by the National Natural Science Foundation of China under Grants U1664257 and U1864201.

Anh-Tu Nguyen, Chouki Sentouh and Jean-Christophe Popieul are with Laboratoire d'Automatique, de Mécanique et d'Informatique industrielles et Humaines (LAMIH UMR CNRS 8201), Université Polytechnique des Hauts-de-France, Valenciennes, France.

Hui Zhang is with the School of Transportation Science and Engineering, Beihang University, Beijing, China.

*Corresponding author (e-mail: nguyen.tranhanhtu@gmail.com).

This paper is concerned with the path following control of autonomous ground vehicles. This typical motion control issue aims at designing steering control laws to reach and follow a desired path without a specific temporal specification [4]. Path following control for autonomous vehicles has received increasing attention, see [3], [5]–[10] and references therein. Using two independent PID nested loops, a vision-based lane keeping controller with successful experimental validation on roads with unknown curvature is proposed in [11]. A recent survey with a special focus on motion planning and feedback control of self-driving urban vehicles is presented in [3], in which a selection of control techniques are discussed, *e.g.*, pure pursuit, feedback linearization, control Lyapunov design, model predictive control (MPC). The authors in [12] provide an interesting analysis to highlight the advantages and drawbacks of three lateral controllers based on sliding mode control, immersion and invariance principle, and system passivity property. Another prominent comparative study between three controllers, including PID, linear-quadratic-Gaussian, and \mathcal{H}_∞ , on their performance limits and tradeoffs (in terms of lane tracking, stability robustness, and passenger comfort) is recently presented in [13]. In addition, obstacle-avoidance control is of crucial importance for autonomous vehicles. A two-stage nonlinear nonconvex control approach, consisting of an outer-loop nonlinear MPC and an inner-loop linear feedback control, is developed for obstacle avoidance in [14]. The authors in [15] develop a combined longitudinal-lateral control strategy for automated vehicle guidance where a nonlinear MPC technique is used for lateral control and the longitudinal speed tracking is guaranteed by another Lyapunov-based control law. Note that various other MPC-based control schemes have been applied to the path following and obstacle avoidance of autonomous vehicles [5], [16]–[18]. However, MPC technique requires solving online optimizations which leads to heavy computational burden, especially for nonlinear MPC problems as highlighted in [16]. Moreover, most of available results on vehicle path following control require *full* state-information for feedback designs. However, due to the excessive cost of vehicle sensors, the measurements of some vehicle states are not available on series-production vehicles, for instance the lateral speed and/or the sideslip angle [19], [20]. In this practical situation, an output feedback control scheme must be used [21]–[23]. It is stressed that output feedback MPC scheme is still an open-ended issue for which a moving horizon estimation must be considered [24].

For engineering applications, the transient behaviors of the closed-loop systems should be carefully studied since stability property is generally not sufficient for practical performance. It is well known that the closed-loop transient response of a linear system is related to the location of its poles. This fact was generalized to LMI (or \mathcal{D} -stability) regions for \mathcal{H}_∞ control design in [25]. The effectiveness of the \mathcal{D} -stability concept to improve the closed-loop transient response has been proved through a large range of control engineering systems, e.g., lateral vehicle dynamics [7], Diesel engine aftertreatment systems [26], etc. Despite numerous successful real-world applications, only few results on \mathcal{D} -stability for vehicle path following control are available, especially when using output feedback control schemes.

Motivated by the above theoretical and practical issues, we propose a novel robust \mathcal{H}_2 static output feedback (SOF) control scheme for path following of autonomous vehicles. In particular, this \mathcal{H}_2 control design fully exploits the \mathcal{D} -stability concept to improve the transient performance of the closed-loop vehicle system, thus the comfort of passengers. Note that the design of SOF controllers using \mathcal{D} -stability is NP-hard [27], and still widely open in the literature. Indeed, most of control applications, especially in intelligent automotive systems, are based on dynamic output feedback schemes [28]–[30]. Such a control scheme may induce complexity/difficulty in real-time implementation. To overcome this drawback, SOF control approaches were also proposed for vehicle path following in [4], [31], in which \mathcal{D} -stability was not considered. Note that the effects of the road curvature was not appropriately taken into account via the \mathcal{H}_2 SOF control design in [31]. Moreover, it may be hard to achieve *practically* a desirable path following performance with the approach in [4] due to the use of a genetic algorithm for the design procedure and the excessive number of linear submodels of the vehicle polytopic system. The contributions of this paper are summarized below.

- 1) Takagi-Sugeno (T-S) fuzzy control technique [32], [33] is exploited to take into account the *time-varying* nature of the vehicle speed. The physical bounds of the speed and the acceleration are explicitly considered in the control design to reduce the conservatism.
- 2) The proposed fuzzy SOF control method allows achieving practical performance on both: (1) closed-loop transient response to improve the passengers' comfort via \mathcal{D} -stability concept, and (2) vehicle path following under unknown road curvatures via a new \mathcal{H}_2 design based on a conceptual T-S fuzzy *standard model*. Using Lyapunov stability arguments, the \mathcal{H}_2 control design is reformulated as an LMI-based optimization problem, efficiently solved with convex semidefinite programming [34]. The proposed SOF control framework can be also applied to a large class of real-world applications.
- 3) The obtained control results are both *theoretically* and *practically* verified with relevant illustrations. To the best of our knowledge, experimental validations of \mathcal{H}_2 T-S fuzzy SOF control for path following of autonomous vehicles have not been reported in the open literature.

The paper is organized as follows. Section II presents the

vehicle nonlinear dynamics and defines the control goals. In Section III, a standard model is formulated for \mathcal{H}_2 control design. Using the \mathcal{D} -stability concept, Section IV discusses the new \mathcal{H}_2 SOF control design for T-S fuzzy systems which is applied later to the path following control. Section V provides experimental results to show the interests of the proposed method. Concluding remarks are drawn in Section VI.

Notation: Ω_N denotes the set $\{1, 2, \dots, N\}$. \mathbb{R} (respectively \mathbb{C}) is the field of real (respectively complex) numbers. I denotes the identity matrix of appropriate dimension. For a matrix X , X^\top indicates its transpose. For any square matrix X , $X \succ 0$ indicates a positive definite matrix, and $\text{He}X = X + X^\top$. $\text{diag}(X_1, X_2)$ denotes a block-diagonal matrix composed of X_1, X_2 . The symbol \star stands for matrix blocks that can be deduced by symmetry. \otimes denotes the Kronecker product of matrices. The argument of a function is omitted when its meaning is clear.

II. VEHICLE MODELING AND PROBLEM STATEMENT

This section reviews the vehicle modeling for lateral control purposes. The vehicle notation is given in Table I.

TABLE I
VEHICLE PARAMETERS

| Notation | Description |
|----------|---|
| M | Vehicle mass [kg] |
| l_f | Distance from the GC to front axle [m] |
| l_r | Distance from the GC to rear axle [m] |
| l_w | Distance from GC to wind impact point [m] |
| l_s | Look-ahead distance [m] |
| η_t | Tire length contact [m] |
| I_z | Inertia of vehicle yaw moment [kgm ²] |
| C_f | Front cornering stiffness [N/rad] |
| C_r | Rear cornering stiffness [N/rad] |
| f_w | Lateral wind force [N] |
| v_x | Vehicle longitudinal speed [m/s] |
| v_y | Vehicle lateral speed [m/s] |
| r | Vehicle yaw rate [rad/s] |
| δ | Vehicle steering angle [rad] |

A. Nonlinear Vehicle Dynamics

A nonlinear single track model is used to represent the vehicle motions, see Fig. 1. This model captures the essential vehicle dynamics which is described as follows [11], [35]:

$$\begin{aligned} M(\dot{v}_x - rv_y) &= F_{xf} \cos \delta - F_{yf} \sin \delta + F_{xr} \\ M(\dot{v}_y + rv_x) &= F_{xf} \sin \delta + F_{yf} \cos \delta + F_{yr} + f_w \\ I_z \dot{r} &= l_f (F_{xf} \sin \delta + F_{yf} \cos \delta) - l_r F_{yr} + l_w f_w. \end{aligned} \quad (1)$$

The front/rear longitudinal forces F_{xi} and lateral forces F_{yi} are modeled using the following Pacejka's formula [36]:

$$\begin{aligned} F_{ki}(\alpha_i) &= D_i \sin(C_i \arctan \xi_i) \\ \xi_i &= (1 - E_i) B_i \alpha_i + E_i \arctan(B_i \alpha_i) \end{aligned}$$

where $k \in \{x, y\}$ and $i \in \{f, r\}$. The Pacejka parameters B_i , C_i , D_i and E_i depend on the characteristics of the tire, the road and the vehicle operating conditions. The sideslip angles of the front and rear tires are given by

$$\alpha_f = \delta - \arctan\left(\frac{v_y + l_f r}{v_x}\right), \quad \alpha_r = \arctan\left(\frac{l_r r - v_y}{v_x}\right).$$

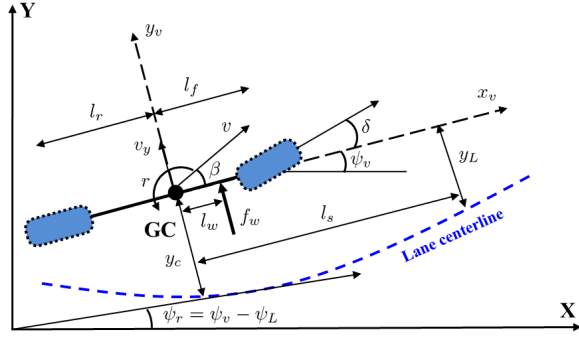


Fig. 1. Lateral vehicle modeling.

Since we focus on the path following, the information on the vehicle position with respect to the lane centerline is required for control design, see Fig. 1. This information can be represented by the lateral error y_L at the look-ahead distance and the heading error ψ_L . The dynamics of these variables are given as [11]

$$\dot{y}_L = \beta v_x + l_s r + \psi_L v_x, \quad \dot{\psi}_L = r - \rho_r v_x \quad (2)$$

where ρ_r is the road curvature.

B. Path Following Control Goals of Autonomous Vehicles

Most of the vehicles are equipped with an inertial navigation system to measure the yaw rate r and an odometer for the measurement of the vehicle speed v_x . The steering angle δ is obtained from an optical encoder. The look-ahead lateral deviation y_L and the heading error ψ_L can be measured by a video camera. The lateral speed v_y and the sideslip angle β can be measured by dual antenna GPS systems or Correvit optical sensors. Unfortunately, due to their excessive costs, the measurements of β and v_y are *unavailable* for real-time implementation in practice [4], [30].

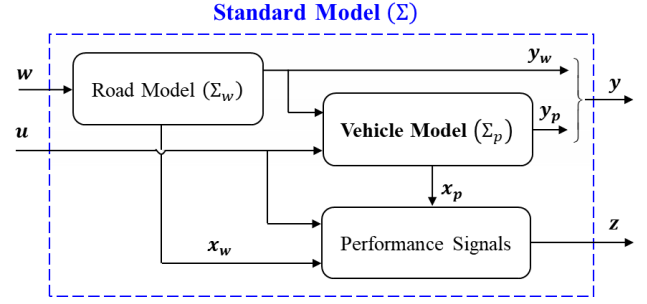
This paper presents a systematic method for path following control which can handle this major practical issue. Specifically, the following design requirements are considered.

- The real-time control implementation can be done with only low-cost sensors of series-production vehicles.
- The control structure must be simple with low numerical complexity for practical application perspective.
- A desirable path following performance with improved transient response is achieved under unknown curvatures.
- The closed-loop control performance and robustness is guaranteed with Lyapunov stability arguments.

To meet these requirements, we propose in Section IV a new fuzzy SOF control design using \mathcal{D} -stability concept.

III. CONTROL-BASED STANDARD MODEL FORMULATION

Based on an \mathcal{H}_2 control scheme, the proposed method makes use of a standard model Σ composed of three following elements: a vehicle model Σ_p , a road model Σ_w , and a model of performance signals, see Fig. 2. Next, we define these three elements to form the corresponding standard model.

Fig. 2. Standard model Σ for \mathcal{H}_2 control design.

A. Control-Based Road-Vehicle Model

For lateral control purposes, the nonlinear vehicle (1) is simplified. The following standard assumptions are considered [37]. First, the longitudinal dynamics and the aerodynamic forces are neglected. Second, the lateral tire forces are proportional to the sideslip angles of each axle. Third, the small angles assumption is used. As a result, the simplified vehicle lateral dynamics is represented by

$$\begin{bmatrix} \dot{\beta} \\ \dot{r} \end{bmatrix} = \begin{bmatrix} a_{11} & a_{12} \\ a_{21} & a_{22} \end{bmatrix} \begin{bmatrix} \beta \\ r \end{bmatrix} + \begin{bmatrix} b_1 \\ b_2 \end{bmatrix} \delta + \begin{bmatrix} e_1 \\ e_2 \end{bmatrix} f_w \quad (3)$$

where the sideslip angle β at the center of gravity (CG) can be computed as $v_y = v_x \sin \beta \simeq v_x \beta$. The elements of the system matrices in (3) are given by

$$\begin{aligned} a_{11} &= -\frac{2(C_r + C_f)}{M v_x}, & a_{12} &= \frac{2(l_r C_r - l_f C_f)}{M v_x^2} - 1, \\ a_{21} &= \frac{2(l_r C_r - l_f C_f)}{I_z}, & a_{22} &= \frac{-2(l_r^2 C_r + l_f^2 C_f)}{I_z v_x}, \\ b_1 &= \frac{2C_f}{M v_x}, & e_1 &= \frac{1}{M v_x}, & b_2 &= \frac{2l_f C_f}{I_z}, & e_2 &= \frac{l_w}{I_z}. \end{aligned}$$

From (2) and (3), the road-vehicle model are obtained as

$$\Sigma_p : \begin{cases} \dot{\mathbf{x}}_p = A_p \mathbf{x}_p + B_p \mathbf{u} + E_{p1} \rho_r + E_{p2} f_w \\ \mathbf{y}_p = C_p \mathbf{x}_p \end{cases} \quad (4)$$

where $\mathbf{x}_p = [\beta \ r \ \psi_L \ y_L]^\top$ is the state vector, \mathbf{y}_p is the measured output, and the steering angle is the control input $\mathbf{u} = \delta$. The system matrices of Σ_p are given by

$$\begin{aligned} A_p &= \begin{bmatrix} a_{11} & a_{12} & 0 & 0 \\ a_{21} & a_{22} & 0 & 0 \\ 0 & 1 & 0 & 0 \\ v_x & l_s & v_x & 0 \end{bmatrix}, & C_p &= \begin{bmatrix} 0 & 1 & 0 & 0 \\ 0 & 0 & 1 & 0 \\ 0 & 0 & 0 & 1 \end{bmatrix} \\ B_p &= [b_1 \ b_2 \ 0 \ 0]^\top, & E_{p1} &= [0 \ 0 \ -v_x \ 0]^\top \\ E_{p2} &= [e_1 \ e_2 \ 0 \ 0]^\top. \end{aligned}$$

The control goal is to guarantee the path following performance of autonomous vehicles under the effects of the road curvature. Hence, the road model should represent the *a priori* knowledge on the curvature. The following generator model is used for the prediction of the curved trajectory:

$$\Sigma_w : \begin{cases} \dot{\mathbf{x}}_w = A_w \mathbf{x}_w + B_w \delta_w \\ \mathbf{y}_w = C_w \mathbf{x}_w \end{cases} \quad (5)$$

where $\mathbf{x}_w = \rho_r$, $A_w = -\frac{1}{\tau_r}$, $B_w = -\frac{1}{\tau_r}$ and $C_w = 1$. The disturbance δ_w is an irreducible signal such as impulse or white noise [38].

Remark 1. Note that the model (5) does not allow for an accurate prediction of a curved trajectory. However, this *predictor* model provides *a priori* information on the dynamics of the road curvature, *i.e.*, via the time constant $\tau_r = 1$ [s]. This latter is reasonable for the prediction of the road curvature in most real-world driving situations. Then, the designed controller can exploit this information to predict and anticipate the system evolution to improve the overall closed-loop behaviors [38], [39]. The model Σ_w can be considered as an input shaping filter. This forbids *discontinuity* corresponding to the assumption that the road is composed of straight segments, circle arcs and clothoids [40]. In particular, for the case of autonomous driving, the introduction of ρ_r in the output \mathbf{y}_w of Σ_w allows incorporating a feedforward control action to improve the path following performance, especially when taking tight curves.

B. Control Performance Specifications

As can be seen later, the upper bound of the closed-loop \mathcal{H}_2 norm should be minimized to improve the control performance. To this end, the performance vector \mathbf{z} should involve variables correlated with the risk of lane departure (*e.g.*, heading error ψ_L and lateral deviation y_L), the driving comfort (*e.g.*, lateral acceleration $a_y \simeq v_x \dot{\beta}$), the energy consumption of the steering system and the comfort of passengers in terms of acceptability (*e.g.*, steering control angle δ), see [37]. Then, the performance vector \mathbf{z} is defined as

$$\mathbf{z} = \mathcal{W} [\psi_L \quad y_L \quad a_y]^\top, \quad \mathcal{W} = \text{diag}(\omega_{\psi_L}, \omega_{y_L}, \omega_{a_y}),$$

where ω_{ψ_L} , ω_{y_L} , ω_{a_y} are the weighting coefficients and

$$\begin{bmatrix} \psi_L \\ y_L \\ a_y \end{bmatrix} = \begin{bmatrix} 0 & 0 & 1 & 0 \\ 0 & 0 & 0 & 1 \\ v_x a_{11} & v_x a_{12} & 0 & 0 \end{bmatrix} \mathbf{x}_p + \begin{bmatrix} 0 \\ 0 \\ v_x b_1 \end{bmatrix} \mathbf{u}.$$

The performance output \mathbf{z} can be rewritten in the form

$$\mathbf{z} = F_p \mathbf{x}_p + G_p \mathbf{u} \quad (6)$$

where

$$F_p = \mathcal{W} \begin{bmatrix} 0 & 0 & 1 & 0 \\ 0 & 0 & 0 & 1 \\ v_x a_{11} & v_x a_{12} & 0 & 0 \end{bmatrix}, \quad G_p = \mathcal{W} \begin{bmatrix} 0 \\ 0 \\ \frac{2C_f}{M} \end{bmatrix}.$$

C. Standard Model for \mathcal{H}_2 Path Following Control

From the definitions of the vehicle model Σ_p in (4), the road model Σ_w in (5) and the performance vector \mathbf{z} in (6), the standard model $\Sigma(v_x)$ ¹ is easily constructed as

$$\Sigma(v_x) : \begin{cases} \dot{\mathbf{x}} = A(v_x)\mathbf{x} + B(v_x)\mathbf{u} + E(v_x)\mathbf{w} \\ \mathbf{z} = F(v_x)\mathbf{x} + G\mathbf{u}, \quad \mathbf{y} = C\mathbf{x} \end{cases} \quad (7)$$

¹The notation $\Sigma(v_x)$ is used to clarify that the system dynamics depends explicitly on the time-varying speed v_x .

where $\mathbf{x}^\top = [\mathbf{x}_p^\top \quad \mathbf{x}_w^\top]$, $\mathbf{y}^\top = [\mathbf{y}_p^\top \quad \mathbf{y}_w^\top]$, $\mathbf{w}^\top = [f_w \quad \delta_w]$

$$A(v_x) = \begin{bmatrix} A_p & E_{p2} \\ 0 & A_w \end{bmatrix}, \quad B(v_x) = \begin{bmatrix} B_p \\ 0 \end{bmatrix}, \quad F(v_x)^\top = \begin{bmatrix} F_p^\top \\ 0 \end{bmatrix}, \\ E(v_x) = \text{diag}(E_{p1}, B_w), \quad C = \text{diag}(C_p, C_w), \quad G = G_p.$$

Note that the premise variables of (7), *i.e.*, v_x , $\frac{1}{v_x}$, $\frac{1}{v_x^2}$, are functions of the vehicle speed which is measured and bounded

$$v_{\min} \leq v_x \leq v_{\max}, \quad v_{\min} = 5 \text{ [m/s]}, \quad v_{\max} = 30 \text{ [m/s]}. \quad (8)$$

Besides the bounds on the vehicle speed given in (8), those of the vehicle acceleration are also given

$$a_{\min} \leq a_x = \dot{v}_x \leq a_{\max}, \quad a_{\max} = -a_{\min} = 4 \text{ [m/s}^2\text{]}. \quad (9)$$

The above *physical* bounds on the longitudinal acceleration represents the limitation of the theoretical kinematic centripetal acceleration of the vehicle [31]. As shown later, a judicious consideration of the bounds given in (8) and (9) in the control design allows reducing the design conservatism.

IV. FUZZY STATIC OUTPUT FEEDBACK CONTROL DESIGN WITH \mathcal{D} -STABILITY CONCEPT

To avoid using costly vehicle sensors while keeping a simple control structure, we present hereafter an LMI-based solution to design \mathcal{H}_2 SOF controllers for T-S fuzzy systems. The concept of \mathcal{D} -stability is exploited to improve the transient performance. The proposed theoretical results are then applied to the path following control of autonomous vehicles.

A. Problem Definition and Preliminaries

For generality, consider a T-S fuzzy system as follows [32]:

$$\Sigma(\theta) : \begin{cases} \dot{\mathbf{x}} = \sum_{i=1}^N \eta_i(\theta) (A_i \mathbf{x} + B_i \mathbf{u} + E_i \mathbf{w}) \\ \mathbf{z} = \sum_{i=1}^N \eta_i(\theta) (F_i \mathbf{x} + G_i \mathbf{u}), \quad \mathbf{y} = \sum_{i=1}^N \eta_i(\theta) C_i \mathbf{x} \end{cases} \quad (10)$$

where $\mathbf{x} \in \mathbb{R}^{n_x}$ is the state, $\mathbf{u} \in \mathbb{R}^{n_u}$ is the control input, $\mathbf{w} \in \mathbb{R}^{n_w}$ is the disturbance, $\mathbf{z} \in \mathbb{R}^{n_z}$ is the controlled output, and \mathbf{y} is the measured output. It is assumed that the premise variable $\theta(t) = [\theta_1(t) \dots \theta_p(t)]^\top$ and its rate of variation $\dot{\theta}(t)$ are smooth and respectively valued in the hypercubes

$$\Theta = \{(\theta_1, \dots, \theta_p)^\top : \theta_j \in [\underline{\theta}_j, \bar{\theta}_j], j \in \Omega_p\}, \\ \Theta_d = \{(\dot{\theta}_1, \dots, \dot{\theta}_p)^\top : \dot{\theta}_j \in [\underline{v}_j, \bar{v}_j], j \in \Omega_p\},$$

where $\underline{\theta}_j \leq \bar{\theta}_j$ (respectively $\underline{v}_j \leq \bar{v}_j$) are *known* bounds on θ_j (respectively $\dot{\theta}_j$), for $j \in \Omega_p$. For conciseness, let us denote $\Pi(\theta) = \sum_{i=1}^N \eta_i(\theta) \Pi_i$, with $\Pi_i \in \{A_i, B_i, E_i, F_i, G_i, C_i\}$, $i \in \Omega_N$. Assume also that the time-varying matrices $\Pi(\theta)$ of (10), with $\Pi \in \{A, B, E, F, G, C\}$, are continuous on the hypercube Θ . The membership functions (MFs) $\eta_i(\theta)$ are continuously differentiable and belong to the simplex

$$\Delta_\theta = \left\{ \eta(\theta) \in \mathbb{R}^N : \sum_{i=1}^N \eta_i(\theta) = 1, \eta_i(\theta) \geq 0, \forall \theta \in \Theta \right\}.$$

Since $(\theta, \dot{\theta}) \in \Theta \times \Theta_d$, the lower bound ϕ_{i1} and the upper bound ϕ_{i2} of $\eta_i(\theta)$ can be easily obtained as follows:

$$\eta_i(\theta) \in [\phi_{i1}, \phi_{i2}], \quad \phi_{i1} \leq \phi_{i2}, \quad i \in \Omega_N. \quad (11)$$

Consider the following fuzzy SOF controller:

$$\mathbf{u} = \sum_{i=1}^N \eta_i(\theta) K_i \mathbf{y} = K(\theta) \mathbf{y}. \quad (12)$$

From (10) and (12), the closed-loop system is represented as

$$\Sigma_{cl}(\theta) : \begin{cases} \dot{\mathbf{x}} = \hat{A}(\theta) \mathbf{x} + E(\theta) \mathbf{w} \\ \mathbf{z} = \hat{F}(\theta) \mathbf{x}, \quad \mathbf{y} = C(\theta) \mathbf{x} \end{cases} \quad (13)$$

where

$$\begin{aligned} \hat{A}(\theta) &= A(\theta) + B(\theta)K(\theta)C(\theta), \\ \hat{F}(\theta) &= F(\theta) + G(\theta)K(\theta)C(\theta). \end{aligned}$$

For engineering applications, the transient behaviors of the closed-loop systems should be studied since guaranteeing only the stability property is not sufficient for practical performance. Here, desirable time response and closed-loop damping are enforced for path following control via \mathcal{D} -stability concept. To this end, LMI regions are defined as follows.

Definition 1 (LMI Regions). A subset \mathcal{D} of the complex plane \mathbb{C} is called an LMI region if there exist a symmetric matrix $\mathbf{X} \in \mathbb{R}^{m \times m}$ and a matrix $\mathbf{Y} \in \mathbb{R}^{m \times m}$ such that

$$\mathcal{D} = \{z \in \mathbb{C} : f_{\mathcal{D}}(z) \prec 0\},$$

with $f_{\mathcal{D}}(z) = \mathbf{X} + z\mathbf{Y} + \bar{z}\mathbf{Y}^{\top}$ and \bar{z} is the complex conjugate of z . Note that the characteristic function $f_{\mathcal{D}}(z)$ takes values in the space of $m \times m$ Hermitian matrices. Some useful LMI regions in control applications include, e.g., α -stability regions, vertical strips, disks, conic sectors [25]. The following lemma guarantees the \mathcal{D} -stability of a matrix \mathbf{A} , i.e., all the eigenvalues of \mathbf{A} are located inside the region \mathcal{D} , see [25].

Lemma 1. A matrix \mathbf{A} is \mathcal{D} -stable if and only if there exists a symmetric matrix \mathbf{P} such that

$$\mathbf{X} \otimes \mathbf{P} + \text{He}(\mathbf{Y} \otimes \mathbf{A}\mathbf{P}) \prec 0, \quad \mathbf{P} \succ 0.$$

As an example, the disk $\mathfrak{D}(\alpha, \mathbf{r})$ of radius \mathbf{r} and center $(-\alpha, 0)$ is an LMI region with the following characteristic function:

$$f_{\mathfrak{D}}(z) = \begin{bmatrix} -\mathbf{r} & \alpha + z \\ \alpha + \bar{z} & -\mathbf{r} \end{bmatrix}. \quad (14)$$

The associated \mathcal{D} -stability of \mathbf{A} is guaranteed if and only if

$$\begin{bmatrix} -\mathbf{r}\mathbf{P} & \alpha\mathbf{P} + \mathbf{A}^{\top}\mathbf{P} \\ \alpha\mathbf{P} + \mathbf{P}\mathbf{A} & -\mathbf{r}\mathbf{P} \end{bmatrix} \prec 0, \quad \mathbf{P} \succ 0. \quad (15)$$

This paper proposes an LMI-based algorithm to deal with the following control problem.

Problem 1. Given a T-S fuzzy system $\Sigma(\theta)$ as in (10) with $\theta(t) \in \Theta$, $\forall t > 0$. Determine the control gains K_i , for $i \in \Omega_N$, such that the SOF controller (12) stabilizes $\Sigma(\theta)$ while

- minimizing the upper bound of the \mathcal{H}_2 -norm $\|\Sigma_{cl}(\theta)\|_2$, specified later, for disturbance attenuation purposes, and
- guaranteeing a desirable transient response of (13) which is predefined through an appropriate LMI region.

For control design, the following parameter-dependent Lyapunov function (PDLF) candidate is considered:

$$\mathbb{V}(\mathbf{x}) = \mathbf{x}^{\top} \left(\sum_{i=1}^N \eta_i(\theta) Q_i \right)^{-1} \mathbf{x} = \mathbf{x}^{\top} Q(\theta)^{-1} \mathbf{x} \quad (16)$$

where $Q_i \succ 0$, for $\forall i \in \Omega_N$. The following result on \mathcal{H}_2 control can be found in [31].

Lemma 2. Consider system $\Sigma_{cl}(\theta)$ defined in (13) with $\theta(t) \in \Theta$, $\forall t > 0$. If there exist a symmetric parameter-dependent matrix $Q(\theta) \in \mathbb{R}^{n_x \times n_x}$, a parameter-dependent matrix $Z(\theta) \in \mathbb{R}^{n_w \times n_w}$, and a scalar $\gamma > 0$ such that

$$\begin{bmatrix} \hat{A}(\theta)Q(\theta) + Q(\theta)\hat{A}(\theta)^{\top} - \dot{Q}(\theta) & \star \\ \hat{F}(\theta)Q(\theta) & -I \end{bmatrix} \prec 0 \quad (17)$$

$$\begin{bmatrix} Z(\theta) & \star \\ E(\theta) & Q(\theta) \end{bmatrix} \succ 0 \quad (18)$$

$$\text{trace}(Z(\theta)) < \gamma^2 \quad (19)$$

Then, the Lyapunov function (16) can be used to prove the stability of (13), and $\|\Sigma_{cl}(\theta)\|_2 < \gamma$ where the \mathcal{H}_2 -norm of the time-varying system $\Sigma_{cl}(\theta)$ is defined as follows [34]:

$$\|\Sigma_{cl}(\theta)\|_2^2 = \lim_{h \rightarrow \infty} \frac{1}{h} \int_0^h \text{trace} \left(\hat{F}(\theta(t))Q(\theta(t))\hat{F}(\theta(t))^{\top} \right) dt.$$

Note that \mathcal{H}_2 control is considered here to achieve a robust path following performance under the time-varying variation of the road curvature. Hence, this is especially interesting to improve the path following control during curve taking.

Remark 2. It is difficult to obtain an effective control solution from Lemma 2 for two reasons. First, the design conditions in Lemma 2 depend on both θ and its time-derivative $\dot{\theta}$. Second, condition (17) is expressed as a *nonlinear* matrix inequality. Based on this lemma, we will present a set of *tractable* conditions to design a fuzzy SOF controller (12).

B. LMI-Based Fuzzy Static Output Feedback Control Design

The following theorem provides conditions to design an SOF controller (12) for T-S fuzzy system (10). To ease the presentation, we assume that $C_i = C$, $\forall i \in \Omega_N$. The case with parameter-dependent output matrix is discussed afterwards.

Theorem 1. Given a T-S fuzzy system in (10) with $\theta(t) \in \Theta$, $\forall t > 0$. If there exist positive definite matrices $Q_i \in \mathbb{R}^{n_x \times n_x}$, matrices $M_i \in \mathbb{R}^{n_u \times n_y}$, $X \in \mathbb{R}^{n_y \times n_y}$, $Z_i \in \mathbb{R}^{n_w \times n_w}$, for $i \in \Omega_N$, and positive scalars γ , ϵ such that

$$\begin{bmatrix} Z_i & \star \\ E_i & Q_i \end{bmatrix} \succ 0 \quad (20)$$

$$\text{trace}(Z_i) < \gamma^2 \quad (21)$$

$$\Xi_{iiklm} \prec 0, \quad \Xi_{ijk lm} + \Xi_{jik lm} \prec 0 \quad (22)$$

for $i, j, k, l \in \Omega_N$, $m \in \Omega_2$, $i < j$ and $k \neq l$. Then, the SOF controller (12) stabilizes the T-S fuzzy system (10) and guarantees that $\|\Sigma(\theta)_{cl}\|_2 < \gamma$. Furthermore, the control feedback gains in (12) are computed as follows:

$$K_i = M_i X^{-1}, \quad i \in \Omega_N. \quad (23)$$

The quantity Ξ_{ijklm} in (22) is defined as

$$\Xi_{ijklm} = \text{He} \begin{bmatrix} \mathcal{X} & 0 & \epsilon B_i M_j \\ G_i M_j C + F_i Q_j & -I/2 & \epsilon G_i M_j \\ C Q_j - X C & 0 & -\epsilon X \end{bmatrix} \quad (24)$$

with $\mathcal{X} = A_i Q_j + B_i M_j C - \phi_{km}(Q_k - Q_l)/2$.

Proof. Multiplying (20) by $\eta_i(\theta) \geq 0$ and summing up for all $i \in \Omega_N$, we obtain (18). Similarly, (21) implies (19). Note that if (22) holds, then $X + X^\top \succ 0$. This guarantees the nonsingularity of X . Since $\eta(\theta) \in \Delta_\theta$, it follows that $\sum_{i=1}^N \dot{\eta}_i(\theta) = 0$. Then, we can easily deduce that

$$\dot{Q}(\theta) = \dot{\eta}_l(\theta) Q_l + \sum_{\substack{k=1 \\ k \neq l}}^N \dot{\eta}_k(\theta) Q_k = \sum_{\substack{k=1 \\ k \neq l}}^N \dot{\eta}_k(\theta) (Q_k - Q_l). \quad (25)$$

For any $\phi_{k1} \leq \dot{\eta}_k(\theta) \leq \phi_{k2}$ in (11), it follows that

$$\dot{\eta}_k(\theta) = \omega_{k1}(\theta) \phi_{k1} + \omega_{k2}(\theta) \phi_{k2}, \quad k \in \Omega_N \quad (26)$$

where $\omega_{k1}(\theta) = \frac{\phi_{k2} - \dot{\eta}_k(\theta)}{\phi_{k2} - \phi_{k1}}$ and $\omega_{k2}(\theta) = \frac{\dot{\eta}_k(\theta) - \phi_{k1}}{\phi_{k2} - \phi_{k1}}$. Clearly, $\omega_{kl}(\theta) \geq 0$ and $\sum_{l=1}^2 \omega_{kl}(\theta) = 1$. From (25) and (26), we get

$$\dot{Q}(\theta) = \sum_{\substack{k=1 \\ k \neq l}}^N \sum_{m=1}^2 \omega_{km}(\theta) \phi_{km} (Q_k - Q_l). \quad (27)$$

Using (24) and (27), inequality (22) implies that

$$\Upsilon_{ii}(\theta) \prec 0, \quad \Upsilon_{ij}(\theta) + \Upsilon_{ji}(\theta) \prec 0 \quad (28)$$

for $i, j \in \Omega_N$, $i < j$, where

$$\Upsilon_{ij}(\theta) = \text{He} \begin{bmatrix} \mathcal{Y}(\theta) & 0 & \epsilon B_i M_j \\ G_i M_j C + F_i Q_j & -I/2 & \epsilon G_i M_j \\ C Q_j - X C & 0 & -\epsilon X \end{bmatrix},$$

and $\mathcal{Y}(\theta) = A_i Q_j + B_i M_j C - \dot{Q}(\theta)/2$. Since $\eta_i(\theta) \geq 0$, $\forall i \in \Omega_N$, it follows from (28) that

$$\begin{aligned} & \sum_{i=1}^N \eta_i(\theta)^2 \Upsilon_{ii}(\theta) + \sum_{i=1}^N \sum_{i < j}^N \eta_i(\theta) \eta_j(\theta) (\Upsilon_{ij}(\theta) + \Upsilon_{ji}(\theta)) \\ &= \sum_{i=1}^N \sum_{j=1}^N \eta_i(\theta) \eta_j(\theta) \Upsilon_{ij}(\theta) \prec 0. \end{aligned} \quad (29)$$

Note that (29) can be rewritten in the form

$$\Phi(\theta) = \begin{bmatrix} \Phi_{11}(\theta) & \star & \star \\ \Phi_{21}(\theta) & -I & \star \\ \Phi_{31}(\theta) & \Phi_{32}(\theta) & -\epsilon(X + X^\top) \end{bmatrix} \prec 0 \quad (30)$$

where

$$\begin{aligned} \Phi_{11}(\theta) &= \text{He}(A(\theta)Q(\theta) + B(\theta)M(\theta)C) - \dot{Q}(\theta), \\ \Phi_{21}(\theta) &= G(\theta)M(\theta)C + F(\theta)Q(\theta), \\ \Phi_{31}(\theta) &= \epsilon M(\theta)^\top B(\theta)^\top + CQ(\theta) - XC, \\ \Phi_{32}(\theta) &= \epsilon M(\theta)^\top D_z(\theta)^\top. \end{aligned}$$

Multiplying (30) with

$$\mathcal{S} = \begin{bmatrix} I & 0 & B(\theta)M(\theta)X^{-1} \\ 0 & I & G(\theta)M(\theta)X^{-1} \end{bmatrix} \quad (31)$$

on the left and its transpose on the right yields (17) after simple manipulations. By Lemma 2, we can conclude the proof. \square

Remark 3. Using the PDLF (16), the information of θ and $\dot{\theta}$ is explicitly considered in the control procedure of Theorem 1 by exploiting the bounds ϕ_{kl} , $k \in \Omega_N$, $l \in \Omega_2$, in (11). This allows reducing the design conservatism. Indeed, if (22) is feasible with an arbitrarily high variation of the MFs, namely

$$\phi_{k1} \rightarrow -\infty, \quad \phi_{k2} \rightarrow +\infty, \quad \forall k \in \Omega_N.$$

Then, it is only possible that $Q_k \approx Q_l$, for $\forall k, l \in \Omega_N$, to minimize the effect of $\phi_{km}(Q_k - Q_l)$ involved in (24). Moreover, if $Q_i = Q$, for $\forall i \in \Omega_N$, in (16). Then, the common quadratic Lyapunov function $V(\mathbf{x}) = \mathbf{x}^\top Q^{-1} \mathbf{x}$ is straightforwardly recovered. This means that Theorem 1 includes precisely the quadratic design results.

Theorem 1 aims to design a stabilizing SOF controller (12) with a guaranteed \mathcal{H}_2 performance. To improve the transient response, it is desirable to take into account the LMI region $\mathfrak{D}(\alpha, \mathbf{r})$, described in Lemma 1, in the design procedure. The following theorem guarantees this \mathcal{D} -stability property.

Theorem 2. Consider the T-S fuzzy system $\Sigma_{cl}(\theta)$ in (13) with $\theta(t) \in \Theta$, $\forall t > 0$. All the eigenvalues of $\hat{A}(\theta)$ are within the LMI region $\mathfrak{D}(\alpha, \mathbf{r})$ if there exist positive definite matrices $\hat{Q}_i \in \mathbb{R}^{n_x \times n_x}$, matrices $M_i \in \mathbb{R}^{n_u \times n_y}$, $X \in \mathbb{R}^{n_y \times n_y}$, for $i \in \Omega_N$, and a positive scalar ϵ such that

$$\Gamma_{ii} \prec 0, \quad \Gamma_{ij} + \Gamma_{ji} \prec 0, \quad i, j \in \Omega_N, \quad i < j \quad (32)$$

where

$$\Gamma_{ij} = \begin{bmatrix} -\mathbf{r}\hat{Q}_j & \star & \star \\ \mathcal{Z}_{ij} & -\mathbf{r}\hat{Q}_j & \star \\ C\hat{Q}_j - XC & \epsilon M_j^\top B_i^\top & -\epsilon(X + X^\top) \end{bmatrix} \quad (33)$$

and $\mathcal{Z}_{ij} = \alpha\hat{Q}_j + A_i\hat{Q}_j + B_i M_j C$.

Proof. Since $\eta_i(\theta) \geq 0$, $\forall i \in \Omega_N$, it follows from (32) that

$$\begin{aligned} & \sum_{i=1}^N \eta_i(\theta)^2 \Gamma_{ii} + \sum_{i=1}^N \sum_{i < j}^N \eta_i(\theta) \eta_j(\theta) (\Gamma_{ij} + \Gamma_{ji}) \\ &= \sum_{i=1}^N \sum_{j=1}^N \eta_i(\theta) \eta_j(\theta) \Gamma_{ij} \prec 0. \end{aligned} \quad (34)$$

With Γ_{ij} defined in (33), inequality (34) can be rewritten as

$$\begin{bmatrix} -\mathbf{r}\hat{Q}(\theta) & \star & \star \\ \mathcal{Z}(\theta) & -\mathbf{r}\hat{Q}(\theta) & \star \\ C\hat{Q}(\theta) - XC & \epsilon M(\theta)^\top B(\theta)^\top & -\epsilon(X + X^\top) \end{bmatrix} \prec 0 \quad (35)$$

where $\mathcal{Z} = \alpha\hat{Q}(\theta) + A(\theta)\hat{Q}(\theta) + B(\theta)M(\theta)C$ and $\hat{Q}(\theta) = \sum_{i=1}^N \eta_i(\theta)\hat{Q}_i$. Multiplying (35) with

$$\mathcal{T} = \begin{bmatrix} I & 0 & 0 \\ 0 & I & B(\theta)M(\theta)X^{-1} \end{bmatrix} \quad (36)$$

on the left and its transpose on the right leads to

$$\begin{bmatrix} -\mathbf{r}\hat{Q}(\theta) & \star \\ [(\alpha + A(\theta) + B(\theta)K(\theta)C)\hat{Q}(\theta) & -\mathbf{r}\hat{Q}(\theta)] \end{bmatrix} \prec 0. \quad (37)$$

By a congruence transformation with $\text{diag}(\hat{Q}(\theta)^{-1}, \hat{Q}(\theta)^{-1})$, (37) is shown to be equivalent to (15) with $\mathbf{P} = \hat{Q}(\theta)^{-1}$ and $\mathbf{A} = \hat{A}(\theta)$. This concludes the proof. \square

The following result provides a solution for Problem 1.

Corollary 1. Given a T-S fuzzy system in (10) with $\theta(t) \in \Theta$, for $\forall t > 0$, and the LMI region $\mathfrak{D}(\alpha, \mathbf{r})$ with the characteristic function (14). If there exist positive definite matrices $Q_i \in \mathbb{R}^{n_x \times n_x}$, $\hat{Q}_i \in \mathbb{R}^{n_x \times n_x}$, matrices $M_i \in \mathbb{R}^{n_u \times n_y}$, $X \in \mathbb{R}^{n_y \times n_y}$, $Z_i \in \mathbb{R}^{n_w \times n_w}$, for $i \in \Omega_N$, and positive scalars γ, ϵ such that

$$\begin{aligned} \min_{\xi_i, i \in \Omega_N} \quad & \gamma^2 \\ \text{s.t.} \quad & (20), (21), (22) \text{ and } (32) \end{aligned} \quad (38)$$

where $\xi_i = (\epsilon, \gamma, Q_i, \hat{Q}_i, M_i, X, Z_i)$. Then, the SOF controller (12) with the control gains in (23) solves Problem 1.

Proof. This is a direct consequence of Theorems 1 and 2. \square

Remark 4. A similar reasoning can be adopted to generalize the result in Corollary 1 to cope with a parameter-dependent output matrix $C(\theta)$. This is accomplished by including the matrices $C_i, i \in \Omega_N$, accordingly in (22).

Remark 5. The extra variable X is introduced in the design conditions of Theorems 1 and 2 via congruence transformations with block-matrices \mathcal{S} and \mathcal{T} defined in (31) and (36). This special feature enables an LMI-based formulation with a single line search parameter for SOF control without requiring any matrix equality constraint and/or matrix rank condition as in most of existing works, see [4], [41] and related references. Such restrictive conditions are hardly tractable with available solvers, especially in T-S fuzzy control framework [23].

Remark 6. The design conditions in Corollary 1 are a set of LMIs with a line search over ϵ . The feedback gains $K_i, i \in \Omega_N$, can be easily computed with YALMIP toolbox [42]. The line search for ϵ was performed with 100 points linearly gridded over a logarithmic scale in $[10^{-5}, 10^5]$.

C. Application to Vehicle Path Following Control

1) *Vehicle fuzzy standard model:* The premise variable vector of system (7) is given as $\theta_* = \left[v_x \quad \frac{1}{v_x} \quad \frac{1}{v_x^2} \right]^\top$. Using the sector nonlinearity approach [32, Chapter 2], the T-S fuzzy representation (10) of the standard model (7) has $2^3 = 8$ linear subsystems. Such a representation leads to conservative results since $v_x, \frac{1}{v_x}$ and $\frac{1}{v_x^2}$ are considered *separately* even they are strongly dependent. To avoid this drawback while significantly reducing the design complexity for real-time implementation, the following variable change is used [30]:

$$v_x = \frac{v_0 v_1}{v_1 + v_0 \theta} \Leftrightarrow \frac{1}{v_x} = \frac{1}{v_0} + \frac{1}{v_1} \theta \quad (39)$$

where $v_0 = \frac{2v_{\min} v_{\max}}{v_{\min} + v_{\max}}$ and $v_1 = \frac{2v_{\min} v_{\max}}{v_{\min} - v_{\max}}$. The new premise variable θ satisfies

$$\theta_{\min} \leq \theta \leq \theta_{\max}, \quad \theta_{\min} = -1, \quad \theta_{\max} = 1. \quad (40)$$

Since $v_x = v_{\min}$ for $\theta = \theta_{\min}$ and $v_x = v_{\max}$ for $\theta = \theta_{\max}$, θ can be used to describe the variation of v_x between its lower and upper bounds. It is easily deduced from (39) that

$$\frac{a_{\min}}{a_0} \leq \dot{\theta} \leq \frac{a_{\max}}{a_0}, \quad a_0 = -\frac{v_0^2}{v_1}. \quad (41)$$

Moreover, applying Taylor's approximation as in [37] to the second expression of (39) leads to

$$v_x \simeq v_0 \left(1 - \frac{v_0}{v_1} \theta \right), \quad \frac{1}{v_x^2} \simeq \frac{1}{v_0^2} \left(1 + 2 \frac{v_0}{v_1} \theta \right). \quad (42)$$

Substituting expressions (39) and (42) into (7) leads to the following vehicle standard model:

$$\Sigma_v(\theta) : \begin{cases} \dot{\mathbf{x}} = A(\theta)\mathbf{x} + B(\theta)\mathbf{u} + E(\theta)\mathbf{w} \\ \mathbf{z} = F(\theta)\mathbf{x} + G\mathbf{u}, \quad \mathbf{y} = C\mathbf{x} \end{cases} \quad (43)$$

which is *linearly* dependent on θ . By the sector nonlinearity approach, $\Sigma_v(\theta)$ defined in (43) can be *exactly* represented in the T-S fuzzy form (10) where

$$\begin{aligned} \Lambda_1 &= \Lambda(\theta_{\min}), & C_1 &= C_2 = C, & \eta_1(\theta) &= (1 - \theta)/2, \\ \Lambda_2 &= \Lambda(\theta_{\max}), & G_1 &= G_2 = G, & \eta_2(\theta) &= (1 + \theta)/2, \end{aligned}$$

and $\Lambda \in \{A, B, E, F\}$.

Remark 7. The variable change (39) allows decreasing the number of parameter vertices from eight to two. This significantly reduces not only the design conservatism but also the numerical complexity of the control structure for real-time implementation. Moreover, given the bounds of θ and $\dot{\theta}$ in (40) and (41), it is straightforward to obtain

$$\phi_{11} \leq \dot{\eta}_1(\theta) \leq \phi_{12}, \quad \phi_{21} \leq \dot{\eta}_2(\theta) \leq \phi_{22},$$

where

$$\phi_{11} = \frac{-a_{\max}}{2a_0}, \quad \phi_{12} = \frac{-a_{\min}}{2a_0}, \quad \phi_{21} = \frac{a_{\min}}{2a_0}, \quad \phi_{22} = \frac{a_{\max}}{2a_0}.$$

2) *Theoretical illustrations:* By Corollary 1, the following control goals can be simultaneously achieved.

- The designed SOF controller stabilizes the vehicle system while minimizing the closed-loop \mathcal{H}_2 norm to guarantee a desirable path following under unknown road curvatures.
- Considering LMI region $\mathfrak{D}(1, 40)$ for control design, the corresponding decay rate and disk constraints enforce a settling time of about 1 [s] for the impulse response and to prevent fast controller dynamics, respectively.

Solving the optimization problem (38), the numerical solver takes 49.96 seconds to provide the following feedback gains:

$$\begin{aligned} K_1 &= [-0.0329 \quad -0.5097 \quad -0.0359 \quad 2.4492], \\ K_2 &= [-0.1072 \quad -0.3118 \quad -0.0348 \quad 3.4798]. \end{aligned}$$

Note that the feedback gains in (and also the Lyapunov matrices which are not given here for brevity) corresponding to two subsystems of the vehicle standard model (43) are significantly different. This also justifies *a posteriori* the interest of using the parameter-dependent controller (12) and the Lyapunov function (16) to improve the closed-loop performance.

Remark 8. The amplitudes of the feedforward gain entries corresponding to the road curvature ρ_r , *i.e.*, $K_{1\rho} = 2.4492$

and $K_{2\rho} = 3.4798$, are significantly important compared to other feedback entries. As highlighted in Section V, this represents the *prediction* capacity of the proposed \mathcal{H}_2 fuzzy SOF controller which is useful to improve the path following performance in case of tight curvatures, see also Remark 1.

We solve the optimization (38) for a fixed decay rate $\alpha = 1$ and different values of the radius r . As expected, the result in Fig. 3 shows that the minimal \mathcal{H}_2 upper bound γ of $\Sigma_v(\theta)$ decreases in function of r . Observe also that no feasible control solution can be found for this real-world application if $r < 26$. It is particularly interesting to note that for the same parameter data, the optimization (38) is *infeasible* for any values of decay rate α and radius r when imposing $Q_1 = Q_2$, *i.e.*, quadratic approach. This clearly demonstrates the advantage of exploiting the vehicle acceleration bounds via the PDLF (16) for the \mathcal{H}_2 T-S fuzzy control design, see Remark 3.

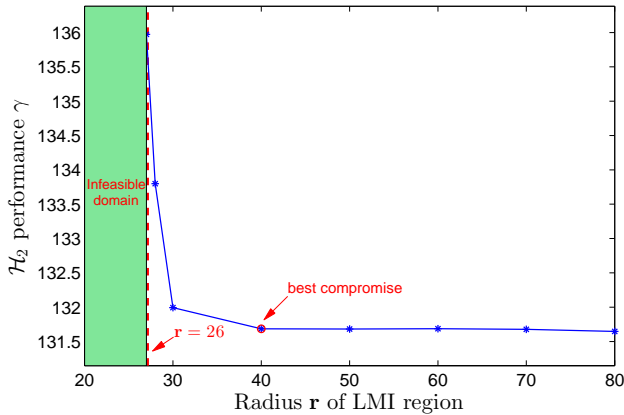


Fig. 3. Minimal \mathcal{H}_2 upper bound of $\Sigma_v(\theta)$ versus r of LMI region $\mathcal{D}(1, r)$.

V. EXPERIMENTAL RESULTS AND DISCUSSIONS

This section presents the experimental results to demonstrate the practical performance of the proposed path following control design. To this end, a series of hardware experiments is conducted under real-world driving situations with a SHERPA simulator. This interactive driving simulator is in the form of a Peugeot 206 vehicle fixed on a Stewart platform, see Fig. 4. The visual is displayed on a 240° wide panoramic screen. This dynamic simulator is structured around a SCANer network connecting fifteen PC-type workstations. All control algorithms were implemented in the SHERPA driving simulator through Matlab/Simulink software.



Fig. 4. (a) SHERPA driving simulator; (b) View of the simulator cockpit.

A. Experiment 1: Real-world Driving with Satory Test Track

This experiment aims to show the path following performance of the designed SOF controller obtained with the database of the Satory track, located 20 km west of Paris, France, see Fig. 5(a). As depicted in Fig. 5(b), this test track is composed of several curved sections including tight bends. The vehicle speed is highly *time-varying* and managed by a human driver during the whole test, see Fig. 5(c). For this real-world driving, observe in Figs. 5(d), (e), (f) and (g) that the proposed SOF controller provides a good path following performance with small tracking errors and a reasonable steering control angle even in cases of aggressive lateral accelerations (about 5 [m/s²]) when taking tight curves, see Fig. 5(h).

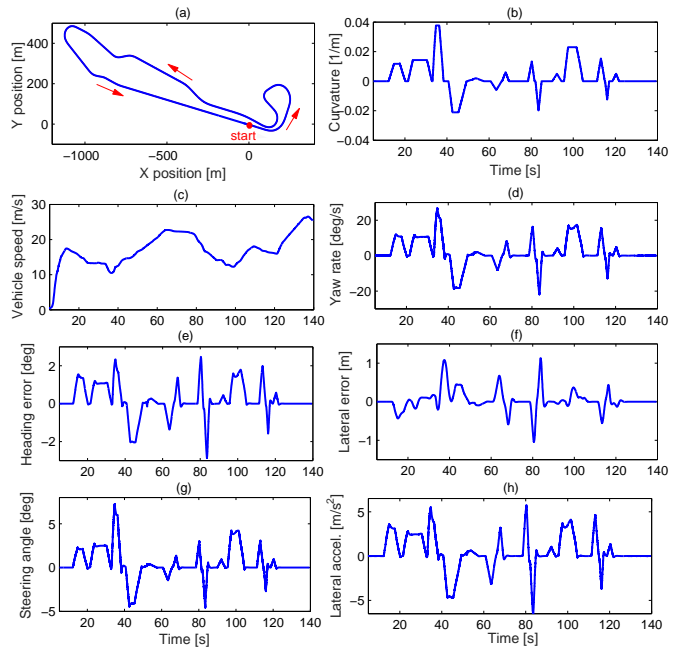


Fig. 5. Automatic path following performed with the Satory test track.

B. Experiment 2: Lane Change Maneuver

To verify the control performance under highly dynamic maneuvering, we assume that the autonomous vehicle must perform a lane change maneuver as illustrated in Fig. 6(a). This driving scenario leads to an important level of lateral acceleration as shown in Fig. 6(f). The vehicle responses obtained with the designed controller, corresponding to three vehicle speeds: $v_x = 30$ [km/h], $v_x = 40$ [km/h], and $v_x = 50$ [km/h], are shown in Fig. 6. Note that since the variation of the vehicle speed is explicitly taken into account in the \mathcal{H}_2 control design, a good path following performance is achieved with the proposed controller for three lane change tests. As expected, although the vehicle responses are quite similar under three different speeds, the tracking errors and the lateral acceleration increase when the vehicle speed becomes more important, see Figs. 6(b), (c), (d) and (f).

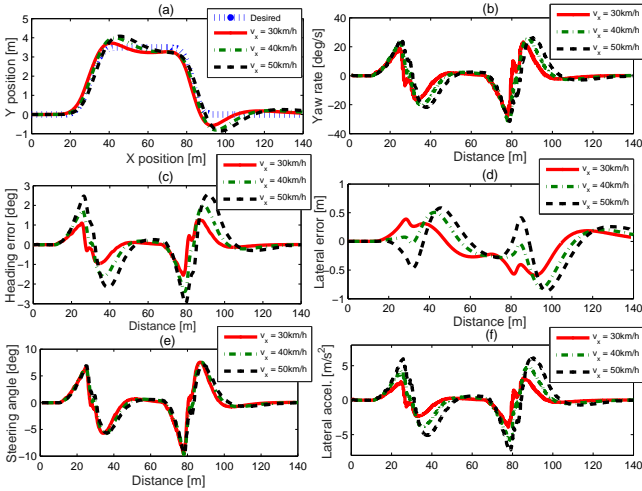


Fig. 6. Vehicle responses with respect to an obstacle avoidance maneuver at different vehicle speeds.

C. Experiment 3: Comparison of Path Following Performance

This test aims to show the interest of using the standard model (7) formalized in Section III for \mathcal{H}_2 control design. To this end, two following T-S fuzzy controllers are compared.

- **Controller 1:** This controller, designed in Section IV-C, is used in previous numerical/experimental experiments.
- **Controller 2:** The only difference of this controller compared to Controller 1 is that for its design, the road model (5) is not taken into account in the formulation of the standard model. Hence, Controller 2 does not have any prediction feature, see Remark 1.

To put in evidence the contribution of the feedforward control action of Controller 1, the two following cases are distinguished for the performance comparison.

1) *Case 1 (Comparison with a constant speed):* For this scenario, the vehicle must perform a path following task at a constant speed $v_x = 70$ [km/h] on a road section composed of small curvatures, see Figs. 7(a) and (b). Fig. 7 shows that a satisfactory performance is achieved with both SOF controllers. However, observe in Fig. 7(e) that the response of Controller 1 is faster than that of the pure feedback Controller 2. This allows Controller 1 to provide a better path following performance than Controller 2, especially in case of high road curvatures as depicted in Figs. 7(c) and (d). Fig. 7(f) represents the feedforward-feedforward control partition of Controller 1. We can see that the feedforward action is always *in advance* compared to the feedback one, and proportional to the road curvature level. This clearly shows the *prediction* capacity of Controller 1 to improve the performance with curved trajectories, see Remark 8.

2) *Case 2 (Comparison with time-varying speed):* The vehicle performs now a driving task as in Case 1 with time-varying vehicle and more important road curvature, see Figs. 8(a) and (b), respectively. Similar to Case 1, Controller 1 provides also a better performance in this case as depicted in Fig. 8. In particular, for the last two curves with a road radius of 100 [m], Controller 2 cannot guarantee any more the path following task, and the vehicle goes out of the road, see

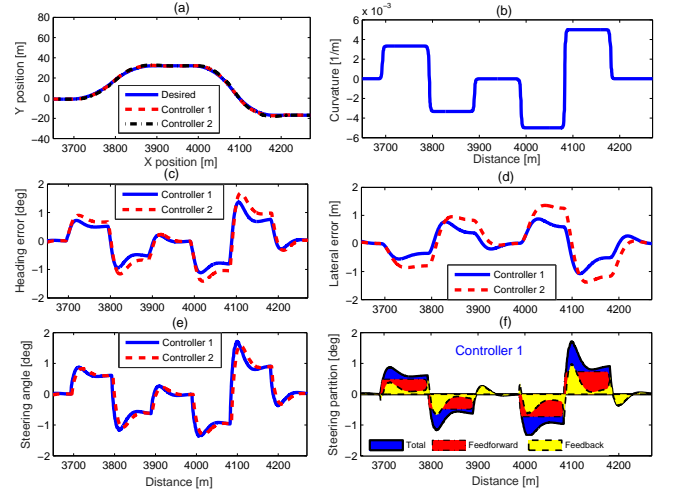


Fig. 7. Comparison of path following performance between two controllers in case of *constant* vehicle speed.

Figs. 8(c), (d), (e) and (f). This emphasizes the interest of the proposed \mathcal{H}_2 control design for path following of autonomous vehicles in various real-world driving conditions.

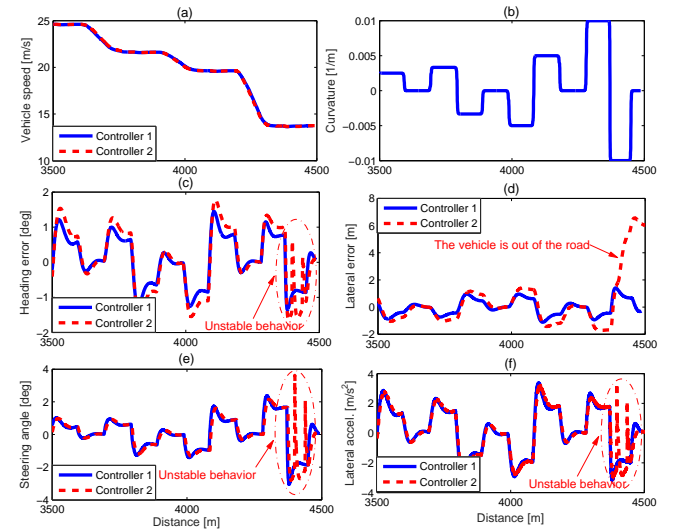


Fig. 8. Comparison of path following performance between two controllers in case of *time-varying* vehicle speed.

VI. CONCLUDING REMARKS

A new LMI-based method to design a path following controller for autonomous ground vehicles has been proposed. The \mathcal{H}_2 control design is formulated based on a conceptual standard vehicle model. To consider the time-varying nature of the vehicle speed, this standard model is transformed into a Takagi-Sugeno fuzzy system with a reduced level of numerical complexity. The proposed \mathcal{H}_2 SOF controller is of the simplest structure and only requires low-cost vehicle sensors for real-time implementation. In particular, the \mathcal{D} -stability concept is exploited to improve the closed-loop transient performance. Moreover, the physical bounds on the vehicle speed and acceleration are judiciously taken into account in

the \mathcal{H}_2 design via a parameter-dependent Lyapunov function to reduce the conservatism. The effectiveness of the new method is demonstrated through hardware experiments under various realistic driving conditions. In particular, the interest of the prediction feature of the proposed SOF controller is clearly put in evidence through appropriate comparisons with experimental results. Future works focus on the application of the proposed SOF control scheme to the driver-automation shared control issue [37].

REFERENCES

- [1] A. Broggi, P. Medici, P. Zani, A. Coati, and M. Panciroli, "Autonomous vehicles control in the VisLab intercontinental autonomous challenge," *Annu. Rev. Control*, vol. 36, no. 1, pp. 161–171, Apr. 2012.
- [2] L. Li, D. Wen, N.-N. Zheng, and L.-C. Shen, "Cognitive cars: A new frontier for ADAS research," *IEEE Trans. Intell. Transp. Syst.*, vol. 13, no. 1, pp. 395–407, Mar. 2012.
- [3] B. Paden, M. Čáp, S. Z. Yong, D. Yershov, and E. Frazzoli, "A survey of motion planning and control techniques for self-driving urban vehicles," *IEEE Trans. Intell. Veh.*, vol. 1, no. 1, pp. 33–55, Mar. 2016.
- [4] C. Hu, H. Jing, R. Wang, F. Yan, and M. Chadli, "Robust \mathcal{H}_∞ output-feedback control for path following of autonomous ground vehicles," *Mech. Syst. Signal Process.*, vol. 70–71, pp. 414–427, Mar. 2016.
- [5] P. Falcone, F. Borrelli, J. Asgari, H. E. Tseng, and D. Hrovat, "Predictive active steering control for autonomous vehicle systems," *IEEE Trans. Control Syst. Technol.*, vol. 15, no. 3, pp. 566–580, May 2007.
- [6] S. Son, W. Kim, S. Lee, and C. Chung, "Robust multirate control scheme with predictive virtual lanes for lane-keeping system of autonomous highway driving," *IEEE Trans. Veh. Technol.*, vol. 64, no. 8, pp. 3378–3391, Aug. 2015.
- [7] J. Wang, G. Zhang, R. Wang, S. C. Schnelle, and J. Wang, "A gain-scheduling driver assistance trajectory-following algorithm considering different driver steering characteristics," *IEEE Trans. Intell. Transp. Syst.*, vol. 18, no. 5, pp. 1097–1108, May 2017.
- [8] X. Li, Z. Sun, D. Cao, D. Liu, and H. He, "Development of a new integrated local trajectory planning and tracking control framework for autonomous ground vehicles," *Mech. Syst. Signal Process.*, vol. 87, pp. 118–137, Mar. 2017.
- [9] M. Brown, J. Funke, S. Erlien, and J. C. Gerdes, "Safe driving envelopes for path tracking in autonomous vehicles," *Control Eng. Pract.*, vol. 61, pp. 307–316, Apr. 2017.
- [10] L. Menhour, B. d'Andréa Novel, M. Fliess, D. Gruyer, and H. Mounier, "An efficient model-free setting for longitudinal and lateral vehicle control: Validation through the interconnected Pro-SiVIC/RTMaps prototyping platform," *IEEE Trans. Intell. Transp. Syst.*, vol. 19, no. 2, pp. 461–475, Feb. 2018.
- [11] R. Marino, S. Scalzi, and M. Netto, "Nested PID steering control for lane keeping in autonomous vehicles," *Control Eng. Pract.*, vol. 19, no. 12, pp. 1459–1467, Dec. 2011.
- [12] G. Tagne, R. Talj, and A. Charara, "Design and comparison of robust nonlinear controllers for the lateral dynamics of intelligent vehicles," *IEEE Trans. Intell. Transp. Syst.*, vol. 17, no. 3, pp. 796–809, Mar. 2016.
- [13] K. Lee, S. E. Li, and D. Kum, "Synthesis of robust lane keeping systems: Impact of controller and design parameters on system performance," *IEEE Trans. Intell. Transp. Syst.*, pp. 1–13, Oct. 2018.
- [14] U. Rosolia, S. De Bruyne, and A. G. Alleyne, "Autonomous vehicle control: A nonconvex approach for obstacle avoidance," *IEEE Trans. Control Syst. Technol.*, vol. 25, no. 2, pp. 469–484, Mar. 2017.
- [15] R. Attia, R. Orjuela, and M. Basset, "Combined longitudinal and lateral control for automated vehicle guidance," *Vehicle Syst. Dyn.*, vol. 52, no. 2, pp. 261–279, Jan. 2014.
- [16] E. Kayacan, H. Ramon, and W. Saeys, "Robust trajectory tracking error model-based predictive control for unmanned ground vehicles," *IEEE/ASME Trans. Mechatron.*, vol. 21, no. 2, pp. 806–814, Apr. 2016.
- [17] J. Funke, M. Brown, S. M. Erlien, and J. C. Gerdes, "Collision avoidance and stabilization for autonomous vehicles in emergency scenarios," *IEEE Trans. Control Syst. Technol.*, vol. 25, no. 4, pp. 1204–1216, July 2017.
- [18] J. Suh, H. Chae, and K. Yi, "Stochastic model predictive control for lane change decision of automated driving vehicles," *IEEE Trans. Veh. Technol.*, vol. 67, no. 6, pp. 4771–4782, June 2018.
- [19] K. Nam, S. Oh, H. Fujimoto, and Y. Hori, "Estimation of sideslip and roll angles of electric vehicles using lateral tire force sensors through RLS and Kalman filter approaches," *IEEE Trans. Ind. Electron.*, vol. 60, no. 3, pp. 988–1000, Mar. 2013.
- [20] B. Zhang, H. Du, J. Lam, N. Zhang, and W. Li, "A novel observer design for simultaneous estimation of vehicle steering angle and sideslip angle," *IEEE Trans. Indus. Electron.*, vol. 63, no. 7, pp. 4357–4366, July 2016.
- [21] A.-T. Nguyen, A. Dequidt, and M. Dambrine, "Anti-windup based dynamic output feedback controller design with performance consideration for constrained Takagi-Sugeno systems," *Eng. Appl. Artif. Intell.*, vol. 40, pp. 76–83, Apr. 2015.
- [22] C. Du, C. Yang, F. Li, and W. Gui, "A novel asynchronous control for artificial delayed Markovian jump systems via output feedback sliding mode approach," *IEEE Trans. Syst., Man, Cybern.: Syst.*, vol. 49, no. 2, pp. 364–374, Feb. 2019.
- [23] A.-T. Nguyen, K. Tanaka, A. Dequidt, and M. Dambrine, "Static output feedback design for a class of constrained Takagi-Sugeno fuzzy systems," *J. Franklin Inst.*, vol. 354, no. 7, pp. 2856–2870, May 2017.
- [24] D. Mayne, "Model predictive control: Recent developments and future promise," *Automatica*, vol. 50, no. 12, pp. 2967–2986, Dec. 2014.
- [25] M. Chilali and P. Gahinet, " \mathcal{H}_∞ design with pole placement constraints: an LMI approach," *IEEE Trans. Autom. Control*, vol. 41, no. 3, pp. 358–367, Mar. 1996.
- [26] H. Zhang and J. Wang, "Improved NO and NO_2 concentration estimation for a Diesel engine aftertreatment system," *IEEE/ASME Trans. Mechatron.*, vol. 23, no. 1, pp. 190–199, Feb. 2018.
- [27] M. Fu, "Pole placement via static output feedback is NP-hard," *IEEE Trans. Autom. Control*, vol. 49, no. 5, pp. 855–857, May 2004.
- [28] H. Li, X. Jing, and H. R. Karimi, "Output-feedback-based \mathcal{H}_∞ control for vehicle suspension systems with control delay," *IEEE Trans. Indus. Electron.*, vol. 61, no. 1, pp. 436–446, Jan. 2014.
- [29] J. Wang, M. Dai, G. Yin, and N. Chen, "Output-feedback robust control for vehicle path tracking considering different human drivers' characteristics," *Mechatronics*, vol. 50, pp. 402–412, Apr. 2018.
- [30] A.-T. Nguyen, C. Sentouh, and J.-C. Popieul, "Sensor reduction for driver-automation shared steering control via an adaptive authority allocation strategy," *IEEE/ASME Trans. Mechatron.*, vol. 23, no. 1, pp. 5–16, Feb. 2018.
- [31] A.-T. Nguyen, P. Chevrel, and F. Claveau, "On the effective use of vehicle sensors for automatic lane keeping via LPV static output feedback control," *IFAC-PapersOnLine*, vol. 50, no. 1, pp. 13 808–13 815, July 2017.
- [32] K. Tanaka and H. Wang, *Fuzzy Control Systems Design and Analysis: a Linear Matrix Inequality Approach*. Wiley-Interscience, 2004.
- [33] A.-T. Nguyen, T. Taniguchi, L. Eciolaza, V. Campos, R. Palhares, and M. Sugeno, "Fuzzy control systems: Past, present and future," *IEEE Comput. Intell. Mag.*, vol. 14, no. 1, pp. 56–68, Feb. 2019.
- [34] S. Boyd, L. El Ghaoui, E. Feron, and V. Balakrishnan, *Linear Matrix Inequalities in System and Control Theory*. SIAM, 1994, vol. 15.
- [35] A.-T. Nguyen, C. Sentouh, and J.-C. Popieul, "Fuzzy steering control for autonomous vehicles under actuator saturation: Design and experiments," *J. Franklin Inst.*, vol. 355, no. 18, pp. 9374–9395, Dec. 2018.
- [36] L. Li, F.-Y. Wang, and Q. Zhou, "Integrated longitudinal and lateral tire/road friction modeling and monitoring for vehicle motion control," *IEEE Trans. Intell. Transp. Syst.*, vol. 7, no. 1, pp. 1–19, 2006.
- [37] A.-T. Nguyen, C. Sentouh, and J.-C. Popieul, "Driver-automation cooperative approach for shared steering control under multiple system constraints: Design and experiments," *IEEE Trans. Ind. Electron.*, vol. 64, no. 5, pp. 3819–3830, May 2017.
- [38] P. Chevrel, in *Analysis and Control of Linear Systems*, P. Larminat, Ed. Wiley-ISTE, 2013, no. 978-1-118-61385-6, ch. Methodology of the State Approach Control, pp. 55–76.
- [39] A.-T. Nguyen, P. Chevrel, and F. Claveau, "LPV static output feedback for constrained direct tilt control of narrow tilting vehicles," *IEEE Trans. Control Syst. Technol.*, pp. 1–10, 2018. [Online]. Available: <https://ieeexplore.ieee.org/abstract/document/8571182>
- [40] E. D. Dickmanns, *Dynamic Vision for Perception and Control of Motion*. Springer Science & Business Media, 2007.
- [41] A.-T. Nguyen, P. Chevrel, and F. Claveau, "Gain-scheduled static output feedback control for saturated LPV systems with bounded parameter variations," *Automatica*, vol. 89, pp. 420–424, Mar. 2018.
- [42] J. Löfberg, "YALMIP: A toolbox for modeling and optimization in Matlab," in *IEEE Int. Symp. Comput. Aided Control Syst. Des.*, Tapei, 2004, pp. 284–289.



Anh-Tu Nguyen is an Associate Professor at the Université Polytechnique des Hauts-de-France, Valenciennes, France. He received the degree in engineering and the M.Sc. degree in automatic control from Grenoble Institute of Technology, France, in 2009, and the Ph.D. degree in automatic control from the University of Valenciennes, France, in 2013.

After working a short period in 2010 at the French Institute of Petroleum, Rueil-Malmaison, France, Dr. Nguyen began his doctoral program at the University of Valenciennes, France, in collaboration with the VALEO Group. From February 2014 to August 2018, Dr. Nguyen was a postdoctoral researcher at the laboratory LAMIH UMR CNRS 8201, Valenciennes, France, and the laboratory LS2N UMR CNRS 6004, Nantes, France. Dr. Nguyen's research interests include robust control, constrained control systems, human-machine shared control for intelligent vehicles.



Jean-Christophe Popieul received the Ph.D. in automatic control from the University of Valenciennes, France, in 1994. He is a Professor of automatic control with the same university, laboratory LAMIH UMR CNRS 8201, Valenciennes, France. Since 1994 his main area of interest is in transport safety. He first focused on driver status assessment, and led several studies dealing with driver vigilance and workload in collaboration with automakers and insurance companies. In 2004 he started to work on ADAS. Beginning with longitudinal driver assistance, he is now working on control sharing for full driving automation.

Prof. Popieul is a member of several scientific boards, including ANR, PREDIT, i-Trans competitiveness cluster, IRT Railenium. He is also leading several Interactive Platforms of LAMIH: SHERPA driving simulator, PSCHITT-Rail train/tram simulator, and PSCHITT-PMR wheelchair simulator.



Chouki Sentouh received the M.Sc. degree from the University of Versailles, Versailles, France, in 2003, and the Ph.D. degree in automatic control from the University of Évry, France, in 2007.

Dr. Sentouh was a postdoctoral researcher from 2007 to 2009 at the laboratory IRCCyN UMR CNRS 6597, Nantes, France. Since 2009, he is an Associate Professor from the University of Valenciennes, Laboratoire d'Automatique, de Mécanique et d'Informatique industrielles et Humaines (LAMIH UMR CNRS 8201), Valenciennes, France. His research interests include automotive control, driver assistance systems with driver interaction, human driver modeling, and cooperation in intelligent transportation systems, shared control for assistance systems.

research interests include automotive control, driver assistance systems with driver interaction, human driver modeling, and cooperation in intelligent transportation systems, shared control for assistance systems.



Hui Zhang is a professor from Beihang University, Beijing, China. He received the B.Sc. degree in mechanical design manufacturing and automation from the Harbin Institute of Technology, China in 2006, the M.Sc. degree in automotive engineering from Jilin University, Changchun, China in 2008, and the Ph.D. degree in mechanical engineering from University of Victoria, Victoria, BC, Canada in 2012.

Dr. Zhang's research interests include Diesel engine aftertreatment systems, vehicle dynamics and control, mechatronics, networked control systems, and multi-agent systems. He is an author/co-author of over 80 peer-reviewed papers on journals. In 2017, he published one book entitled "Modeling, Dynamics, and Control of Electrified Vehicles" with Elsevier Woodhead Publishing.

Dr. Zhang is a recipient of 2017 IEEE Transactions on Fuzzy Systems Outstanding Paper Award and 2018 SAE Ralph R. Teetor Educational Award. He is a member of SAE International, a senior member of IEEE and a member of ASME. Dr. Zhang has served on the IFAC Technical Committee on Automotive Control, ASME Automotive and Transportation Systems Technical Committee. Dr. Zhang serves as an Associate Editor for IEEE Transactions on Vehicular Technology, SAE International Journal of Vehicle Dynamics, Stability, and NVH, SAE International Journal of Connected and Automated Vehicles; Board member of International Journal of Hybrid and Electric Vehicles, Mechanical Systems and Signal Processing; Guest Editor of Mechatronics, IEEE Access, ISA Transactions, Mechanical Systems and Signal Processing, Journal of the Franklin Institute, and International Journal of Vehicle Design; Conference Editorial Board of ASME Dynamic Systems and Control Division, and American Control Conference.